Supplement of Atmos. Chem. Phys., 17, 8923–8938, 2017
https://doi.org/10.5194/acp-17-8923-2017-supplement

Atmospheric Chemistry and Physics
Open Access
EGU

Supplement of

Evaporation of sulfate aerosols at low relative humidity

Georgios Tsagkogeorgas et al.

Correspondence to: Georgios Tsagkogeorgas (george.tsagkogeorgas@tropos.de)

Table S1. Coefficient of determination (R^2) between the modelled and measured geometric mean diameter (GMD) for experiments 1, 2 and 3. Also the simulation number that we refer to in the text, the Case with the corresponding values for the equilibrium coefficients $K_{H_2SO_4,288K}$ and ${}^{x}K_{SO_3,288K}$, the $B_{H_2SO_4}$ and B_{SO_3} values (cf. Eq. 20) to describe the temperature dependence of $K_{H_2SO_4}$ and ${}^{x}K_{SO_3,}$, the assumed species composition of the particle contamination (Con.), and the source to the pure–liquid saturation vapour pressure parameterizations are given.

Exp. No.	Sim. No	Case	$B_{H_2SO_4}$ (K)	B_{SO_3} (K)	$K_{H_2SO_4,288K}$ (mol·kg^{-1})	${}^{x}K_{SO_3,288K}$	Con.	Vap. pres.	R^2
1	1	[a]1	0	0	$2.00 \cdot 10^{9}$	∞	NH_3	N–K–L, Nickless	0.994
1	2	[b]2a	0	0	$2.40 \cdot 10^{9}$	$1.43 \cdot 10^{10}$	NH_3	N–K–L, Nickless	0.994
1	3	[c]2b	0	0	$4.00 \cdot 10^{9}$	$1.54 \cdot 10^{9}$	NH_3	N–K–L, Nickless	0.996
1	4	[d]3	0	0	$1.00 \cdot 10^{11}$	$3.33 \cdot 10^{7}$	NH_3	N–K–L, Nickless	0.992
1	5	1	0	0	**	∞	Org.	N–K–L, Nickless	0.992
1	6	2a	0	0	$2.40 \cdot 10^{9}$	$1.43 \cdot 10^{10}$	Org.	N–K–L, Nickless	0.995
1	7	2a	0	0	$2.40 \cdot 10^{9}$	$1.43 \cdot 10^{10}$	DMA	N–K–L, Nickless	0.993
1	8	1	0	0	$3.80 \cdot 10^{9}$	∞	NH_3	ASPEN	0.990
1	9	2a	0	0	$4.00 \cdot 10^{9}$	$4.55 \cdot 10^{10}$	NH_3	ASPEN	0.993
1	10	2b	0	0	$5.00 \cdot 10^{9}$	$5.00 \cdot 10^{9}$	NH_3	ASPEN	0.995
1	11	3	0	0	$1.00 \cdot 10^{11}$	$5.00 \cdot 10^{7}$	NH_3	ASPEN	0.990
1	12	1	0	0	**	∞	Org.	ASPEN	0.888
2	13	1	0	0	$2.00 \cdot 10^{9}$	∞	NH_3	N–K–L, Nickless	0.870
2	14	2a	0	0	$2.40 \cdot 10^{9}$	$1.43 \cdot 10^{10}$	NH_3	N–K–L, Nickless	0.869
2	15	2b	0	0	$4.00 \cdot 10^{9}$	$1.54 \cdot 10^{9}$	NH_3	N–K–L, Nickless	0.871
2	16	3	0	0	$1.00 \cdot 10^{11}$	$3.33 \cdot 10^{7}$	NH_3	N–K–L, Nickless	0.868
2	17	2a	0	0	$2.40 \cdot 10^{9}$	$1.43 \cdot 10^{10}$	Org.	N–K–L, Nickless	0.870
2	18	2a	0	0	$2.40 \cdot 10^{9}$	$1.43 \cdot 10^{10}$	DMA	N–K–L, Nickless	0.869
2	19	1	0	0	**	∞	Org.	N–K–L, Nickless	0.868
2	20	1	0	0	$3.80 \cdot 10^{9}$	∞	NH_3	ASPEN	0.867
2	21	2a	0	0	$4.00 \cdot 10^{9}$	$4.55 \cdot 10^{10}$	NH_3	ASPEN	0.870
2	22	2b	0	0	$5.00 \cdot 10^{9}$	$5.00 \cdot 10^{9}$	NH_3	ASPEN	0.871
2	23	3	0	0	$1.00 \cdot 10^{11}$	$5.00 \cdot 10^{7}$	NH_3	ASPEN	0.867
2	24	1	0	0	**	∞	Org.	ASPEN	0.510
3	25	1	0	0	$2.00 \cdot 10^{9}$	∞	NH_3	N–K–L, Nickless	0.841
3	26	1	0	0	$2.00 \cdot 10^{9}$	∞	Org.	N–K–L, Nickless	0.905

3	27	1	3475*	0	$2.00 \cdot 10^{9}$	∞	NH_3	N–K–L, Nickless	0.534
3	28	1	0	0	**	∞	Org.	N–K–L, Nickless	0.967
3	29	2a	3475*	14245.7*	$2.40 \cdot 10^{9}$	$1.43 \cdot 10^{10}$	NH_3	N–K–L, Nickless	0.611
3	30	2a	3475*	0	$2.40 \cdot 10^{9}$	$1.43 \cdot 10^{10}$	NH_3	N–K–L, Nickless	0.825
3	31	2a	3475*	–10000	$2.40 \cdot 10^{9}$	$1.43 \cdot 10^{10}$	NH_3	N–K–L, Nickless	0.992
3	32	2a	0	14245.7*	$2.40 \cdot 10^{9}$	$1.43 \cdot 10^{10}$	NH_3	N–K–L, Nickless	0.839
3	33	2a	0	0	$2.40 \cdot 10^{9}$	$1.43 \cdot 10^{10}$	NH_3	N–K–L, Nickless	0.981
3	34	2a	0	0	$2.40 \cdot 10^{9}$	$1.43 \cdot 10^{10}$	Org.	N–K–L, Nickless	0.991
3	35	2a	0	–10000	$2.40 \cdot 10^{9}$	$1.43 \cdot 10^{10}$	NH_3	N–K–L, Nickless	0.860
3	36	2a	0	–3000	$2.40 \cdot 10^{9}$	$1.43 \cdot 10^{10}$	NH_3	N–K–L, Nickless	0.993
3	37	2b	3475*	14245.7*	$4.00 \cdot 10^{9}$	$1.54 \cdot 10^{9}$	NH_3	N–K–L, Nickless	0.937
3	38	2b	3475*	0	$4.00 \cdot 10^{9}$	$1.54 \cdot 10^{9}$	NH_3	N–K–L, Nickless	0.819
3	39	2b	3475*	– 10000	$4.00 \cdot 10^{9}$	$1.54 \cdot 10^{9}$	NH_3	N–K–L, Nickless	0.458
3	40	2b	3475*	5000	$4.00 \cdot 10^{9}$	$1.54 \cdot 10^{9}$	NH_3	N–K–L, Nickless	0.918
3	41	2b	0	14245.7*	$4.00 \cdot 10^{9}$	$1.54 \cdot 10^{9}$	NH_3	N–K–L, Nickless	0.953
3	42	2b	0	0	$4.00 \cdot 10^{9}$	$1.54 \cdot 10^{9}$	NH_3	N–K–L, Nickless	0.685
3	43	2b	0	– 10000	$4.00 \cdot 10^{9}$	$1.54 \cdot 10^{9}$	NH_3	N–K–L, Nickless	0.260
3	44	3	3475*	14245.7*	$1.00 \cdot 10^{11}$	$3.33 \cdot 10^{7}$	NH_3	N–K–L, Nickless	0.903
3	45	3	3475*	0	$1.00 \cdot 10^{11}$	$3.33 \cdot 10^{7}$	NH_3	N–K–L, Nickless	0.571
3	46	3	3475*	– 10000	$1.00 \cdot 10^{11}$	$3.33 \cdot 10^{7}$	NH_3	N–K–L, Nickless	0.146
3	47	3	0	14245.7*	$1.00 \cdot 10^{11}$	$3.33 \cdot 10^{7}$	NH_3	N–K–L, Nickless	0.898
3	48	3	0	0	$1.00 \cdot 10^{11}$	$3.33 \cdot 10^{7}$	NH_3	N–K–L, Nickless	0.420
3	49	3	0	– 10000	$1.00 \cdot 10^{11}$	$3.33 \cdot 10^{7}$	NH_3	N–K–L, Nickless	0.138
3	50	1	0	0	$3.80 \cdot 10^{9}$	∞	NH_3	ASPEN	0.991
3	51	2a	0	0	$4.00 \cdot 10^{9}$	$4.55 \cdot 10^{10}$	NH_3	ASPEN	0.992
3	52	2b	0	0	$5.00 \cdot 10^{9}$	$5.00 \cdot 10^{9}$	NH_3	ASPEN	0.880
3	53	3	0	0	$1.00 \cdot 10^{11}$	$5.00 \cdot 10^{7}$	NH_3	ASPEN	0.540

* Values from Que et al. (2011).

** Simulation with the H_2SO_4 activity derived from Eq. (15) using the thermodynamic data from Giauque et al. (1960)

[a] Case 1: Only evaporation of H_2SO_4.

[b] Case 2a: Both H_2SO_4 and SO_3 evaporate from the particles. H_2SO_4 is the main evaporating species at $T=288.8$ K.

[c] Case 2b: Both H_2SO_4 and SO_3 evaporate from the particles. SO_3 is the main evaporating species at $T=288.8$ K.

[d] Case 3: SO_3 is completely dominating the evaporation.

S1 AMS measurements

The evaporation of sulphate particles based on AMS measurements (Fig. S1 (a)) showed that the particles were composed almost exclusively of sulphuric acid. Calculations of the kappa value κ, based on the AMS measurements, yield a value close to the κ for pure sulphuric acid particles (see Fig. S2).

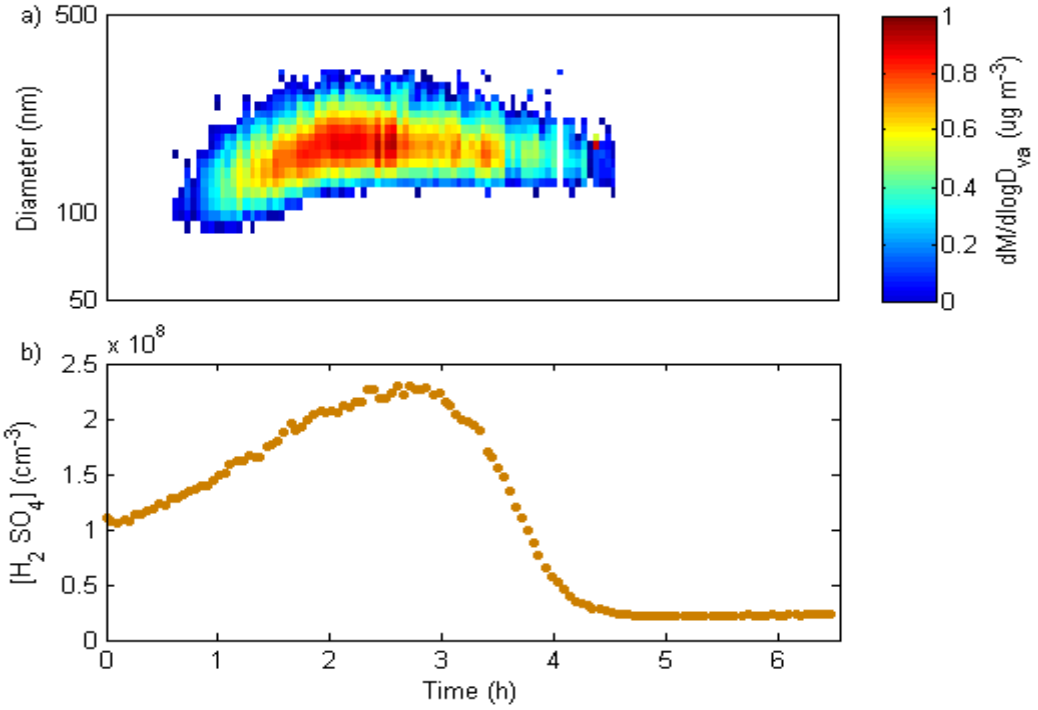

Figure S1. (a) Sulphate mass size distribution ug·m^{-3} (from AMS data) and (b) gas–phase H_2SO_4 concentration (from CIMS data) increases until reaches a peak value during the aerosol particle evaporation experiment 2 performed at *T=288.8* K.

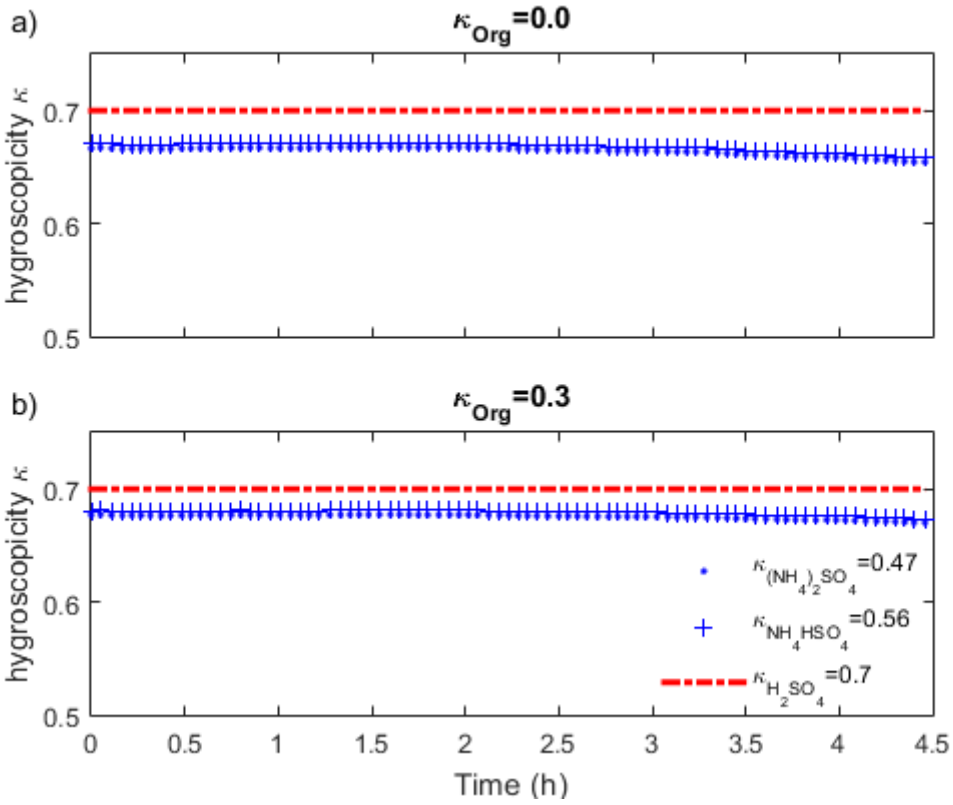

Figure S2. Hygroscopicity kappa (*κ*), based on the AMS measurements, of mixed particles as a function of time for experiment 3. *κ* derived from the hygroscopicities of the components (assumed the lower and higher κ values for bases like ammonium sulphate, $\kappa_{(NH_4)_2SO_4}$*=0.47* and ammonium bisulfate, $\kappa_{NH_4HSO_4}$*=0.56* (Topping et al., 2005; Petters and Kreidenweis 2007), and organics with *O:C=0*, κ_{Org}*=0.0* and *O:C=1*, κ_{Org}*=0.3* (Massoli et al., 2010)) and their respective volume fractions by applying the Zdanovskii–Stokes–Robinson (ZSR) mixing rule. For the calculation of the volume concentration of each compound assumed liquid phase density of SO_4, NH_4, NO_3, Chl, Org constituents (http://cires1.colorado.edu/jimenez–group/wiki). The difference in percentage of *κ* values calculated for the two extreme cases of $\kappa_{(NH_4)_2SO_4}$*=0.47*, $\kappa_{NH_4HSO_4}$*=0.56* is 0.4 %, while for κ_{Org}*=0.0* and κ_{Org}*=0.3* is 1 %. The result shows a *κ* very close to that of pure sulphuric acid (Sullivan et al., 2010).

S2 Mole fraction based activity coefficients of H_2SO_4 and SO_3 and water activity

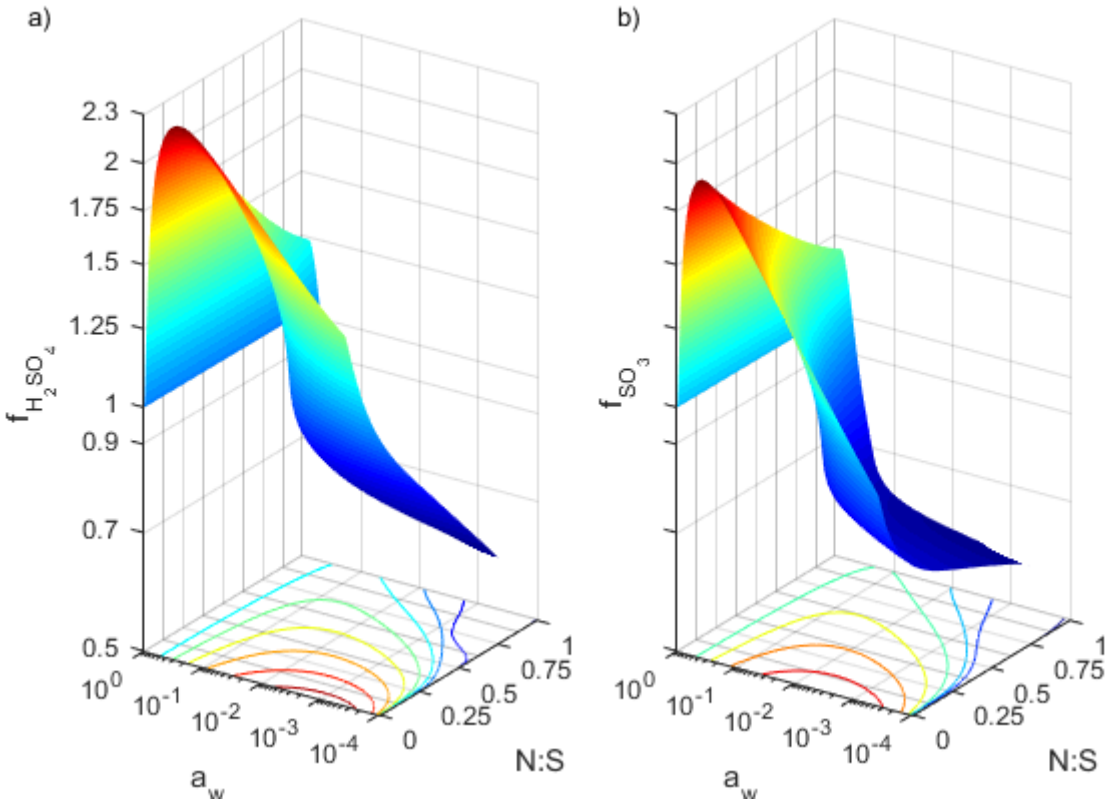

Figure S3. Modelled mole fraction based activity coefficient of (a) H_2SO_4 ($f_{H_2SO_4}$) with equilibrium constant $K_{H_2SO_4}=2.40\cdot10^9$ mol·kg^{-1}, and (b) SO_3 (f_{SO_3}) with equilibrium constant ${}^xK_{SO_3}=1.43\cdot10^{10}$, at $T=288.8$ K, as a function of the water activity, a_w, on the y–axis and $N:S$ on the x–axis. The colour coded contours on x–y axes represent constant activity coefficient for a) $f_{H_2SO_4}=0.8–2.2$ and b) $f_{SO_3}=0.8–1.8$.

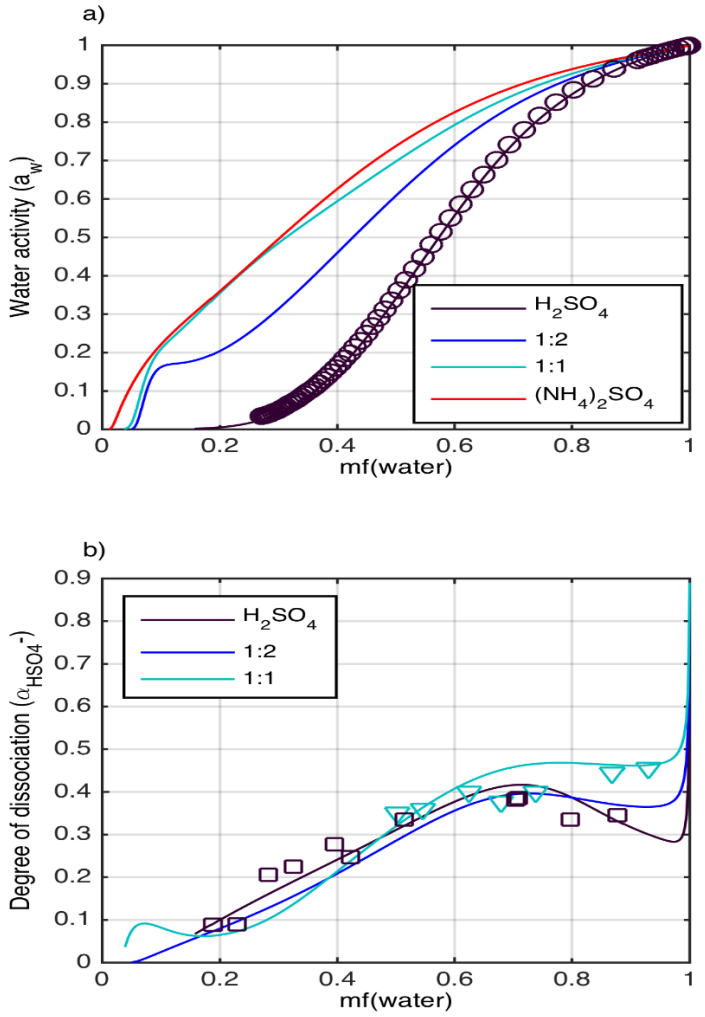

Figure S4. (a) Modelled water activity curves and b) degree of dissociation of HSO_4^- as a function of water mass fraction in aqueous solutions of H_2SO_4 and mixtures of $(NH_4)_2SO_4$ and H_2SO_4. The model simulations and measurements were performed at 298 K. The modelled water activity curves are lines colour coded. The purple curve corresponds to pure sulphuric acid, blue and cyan curves to 1:2 and 1:1 molar ratio of *$(NH_4)_2SO_4$:H_2SO_4* and red curve to pure ammonium sulphate. The measured water activity curve is symbol coded. The purple circle symbol corresponds to $H_2SO_{4(aq)}$ (Staples 1981). (b) the modelled degree of dissociation, $\alpha_{HSO_4^-}$, curves are lines colour coded (corresponding to same aqueous solutions as the curves in Fig. (S4 (a)). The measured degree of dissociation is symbol colour coded (purple squares corresponds to $H_2SO_{4(aq)}$, Myhre et al. (2003), cyan triangles to the 1:1 *$(NH_4)_2SO_4$:H_2SO_4* mixture, Dawson et al. (1986)). The model results can be compared with analogous results in Fig. 10 from Zuend et al., 2011.

S3 Saturation vapour pressure parameterizations

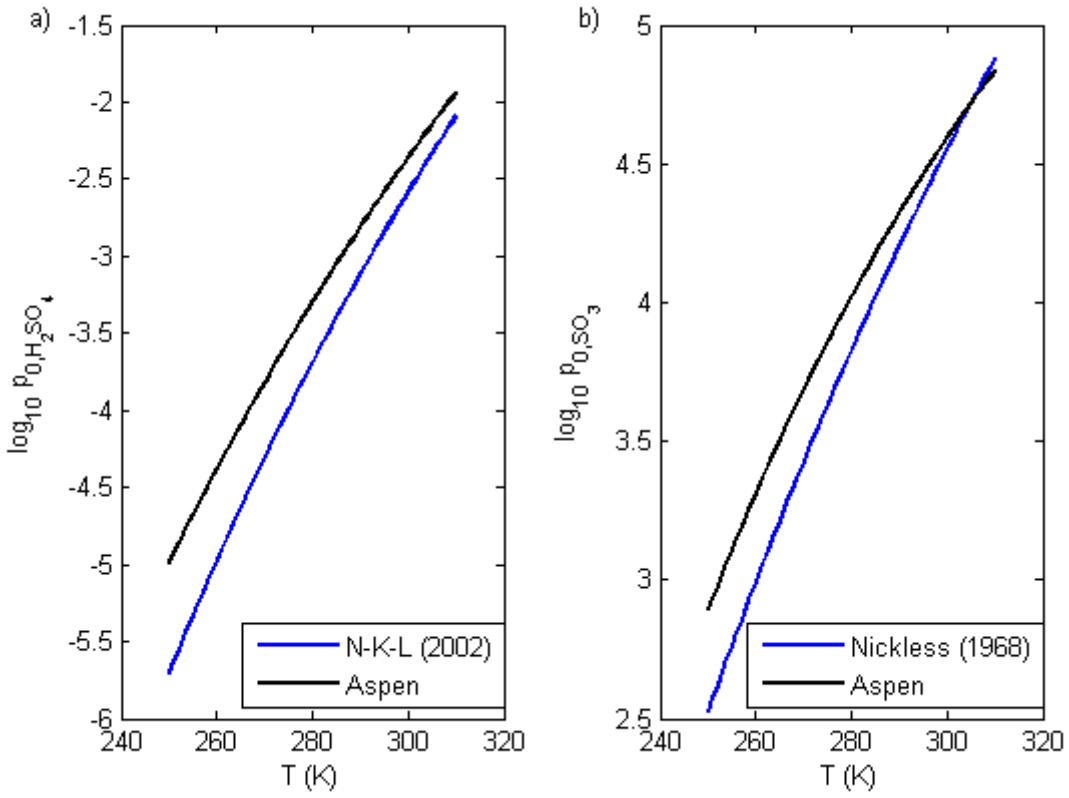

Figure S5. Saturation vapour pressures for H_2SO_4 and SO_3. Comparison among two different pure liquid saturation vapour pressure parameterizations (a) for H_2SO_4 and (b) for SO_3. In panel (a) the blue curve corresponds to the parameterization from the work of Kulmala and Laaksonen (1990), which was optimized by Noppel et al., 2002 (N–K–L parameterization), Eq. (11). The black curve corresponds to the parameterization from Que et al., 2011 (original Aspen Plus Databank). In panel (b) the blue curve corresponds to the parameterization from the work of Nickless (1968), Eq. (12) and the black curve to the parameterization from Que et al., 2011 (original Aspen Plus Databank).

S4 The Kelvin effect

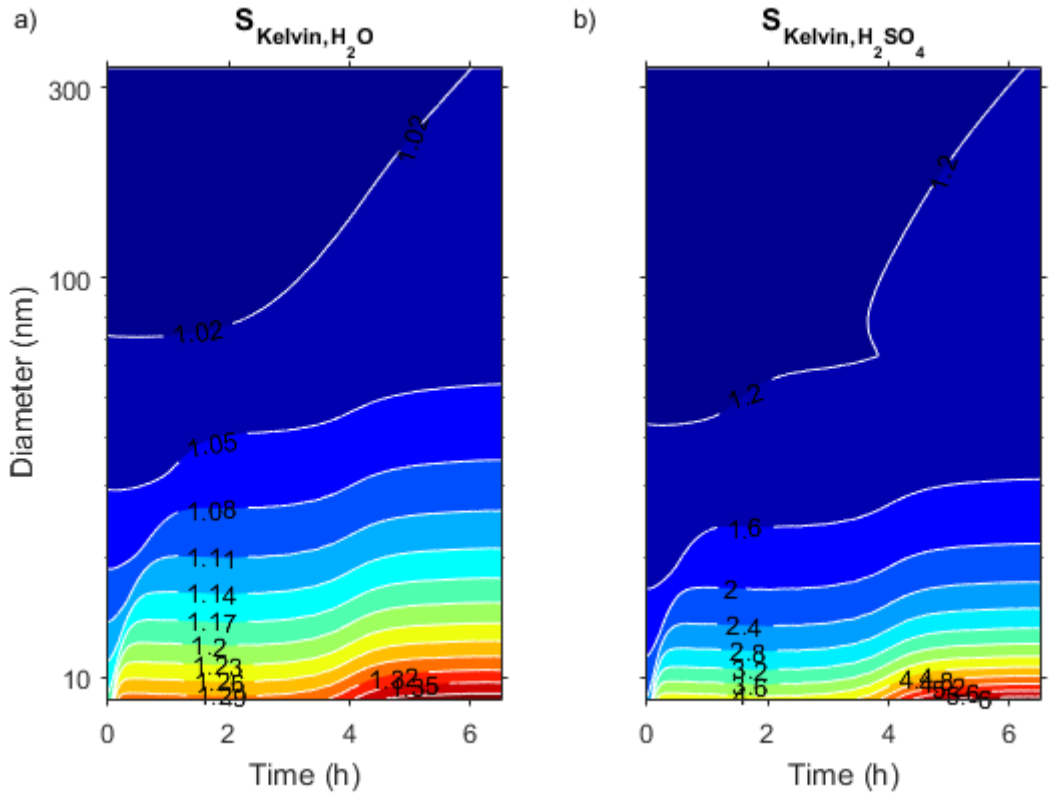

Figure S6. The Kelvin effect for experiment 2 at *T=288.8* K for Case 2a ($K_{H_2SO_4}$=*2.40·10*^{9} mol·kg^{-1} and $^xK_{SO_3}$=*1.43·10*^{10}) illustrates the increase in (a) water (white contours correspond to the Kelvin terms S_{Kelvin,H_2O}=*1.02–1.38*) and (b) H_2SO_4 (white contours represent the Kelvin terms S_{Kelvin,H_2SO_4}=*1.2–6.0*) saturation vapour pressures. The minimum particle size diameter for experiment 2 is ~40 nm, so the maximum value of the Kelvin term is ~1.44 for sulphuric acid.

S5 Saturation concentration of H_2SO_4 and SO_3

We can calculate the saturation concentration of H_2SO_4 ($C_{H_2SO_4,S}$, Eq. S1) and SO_3 ($C_{SO_3,S}$, Eq. S2) in μg·m^{-3} (Fig. S7) with the H_2SO_4 dissociation equilibrium coefficients, $K_{H_2SO_4}=2.4\cdot10^9$ mol·kg^{-1}, and ${}^xK_{SO_3}=1.43\cdot10^{10}$, based on the mole fractions (Fig. 2), the modelled mole fraction based activity coefficients (Fig. S3), the pure liquid saturation vapours pressure parameterizations, Eq. (11) and (12), and the Kelvin effect, Eq. (14).

$$C_{H_2SO_4,S} = \frac{p_{0,H_2SO_4} \cdot x_{H_2SO_4} \cdot f_{H_2SO_4} \cdot C_{k,H_2SO_4}}{R \cdot T \cdot M_{H_2SO_4}} \quad \text{(S1)}$$

$$C_{SO_3,S} = \frac{p_{0,SO_3} \cdot x_{SO_3} \cdot f_{SO_3} \cdot C_{k,SO_3}}{R \cdot T \cdot M_{SO_3}} \quad \text{(S2)}$$

For almost dry conditions ($a_w=3.7\cdot10^{-4}$) and $N{:}S=0$, $C_{H_2SO_4,S}\approx2.6$ μg·m^{-3} and $C_{SO_3,S}\approx8.8$ μg·m^{-3}. However, as long as a_w is larger than $1.3\cdot10^{-3}$, $C_{H_2SO_4,S}$ becomes larger than $C_{SO_3,S}$. Thus, for the conditions during the experiments ($RH>0.3$ %) this thermodynamic setup can be categorized as Case 2a.

With the Aspen Plus Databank pure–liquid saturation vapour pressure parameterization and $K_{H_2SO_4}=4.00\cdot10^9$ mol·kg^{-1} and ${}^xK_{SO_3}=4.55\cdot10^{10}$ $C_{H_2SO_4,S}$ is always higher than $C_{SO_3,S}$ ($C_{H_2SO_4,S}=3.33$ μg·m^{-3} and $C_{SO_3,S}=2.28$ μg·m^{-3} at $a_w=2\cdot10^{-4}$ and $N{:}S=0$). Thus, this model setup can be also classified as Case 2a.

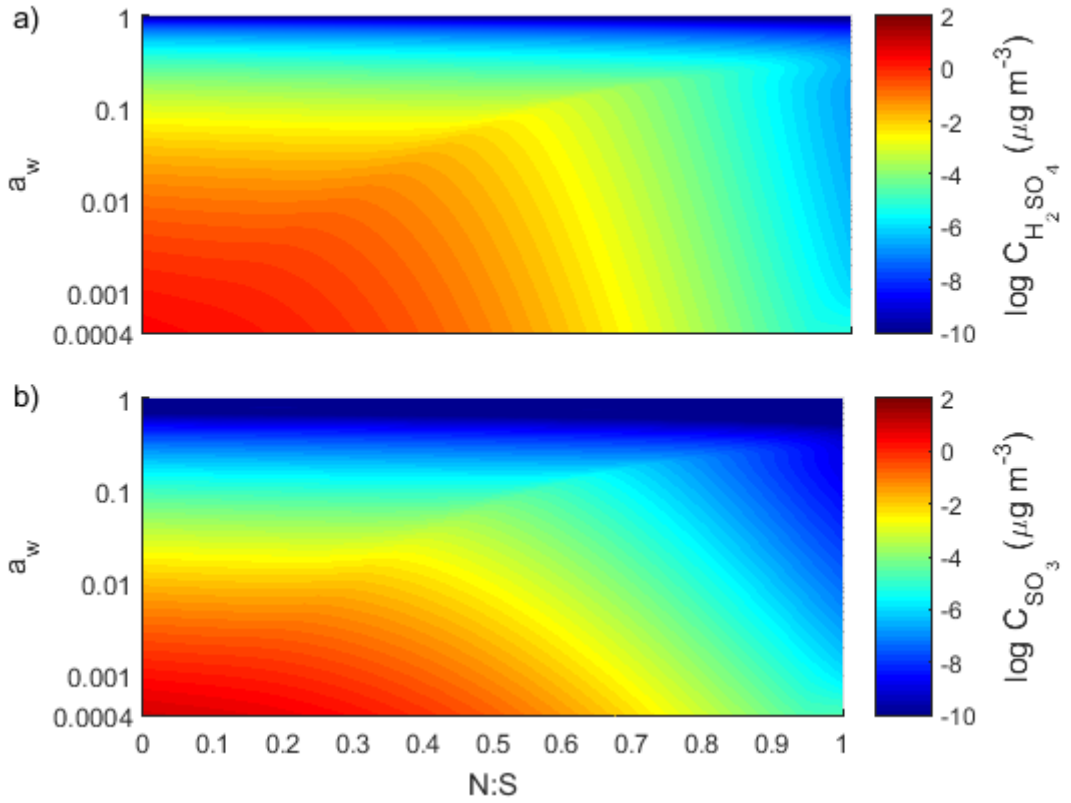

Figure S7.I. (a) The saturation concentration of H_2SO_4 $(C_{H_2SO_4,S})$ and (b) SO_3 $(C_{SO_3,S})$ in µg·m^{-3} as a function of a_w and *N:S* at *T=288.8* K. The H_2SO_4 dissociation equilibrium coefficients are $K_{H_2SO_4}$=*2.4·10^9* mol·kg^{-1}, and $^xK_{SO_3}$=*1.43·10^{10}*. For the H_2SO_4 and SO_3 pure liquid saturation vapour pressures are used the N–K–L, Eq. (11) and Nickless, Eq. (12) parameterisations, respectively.

5

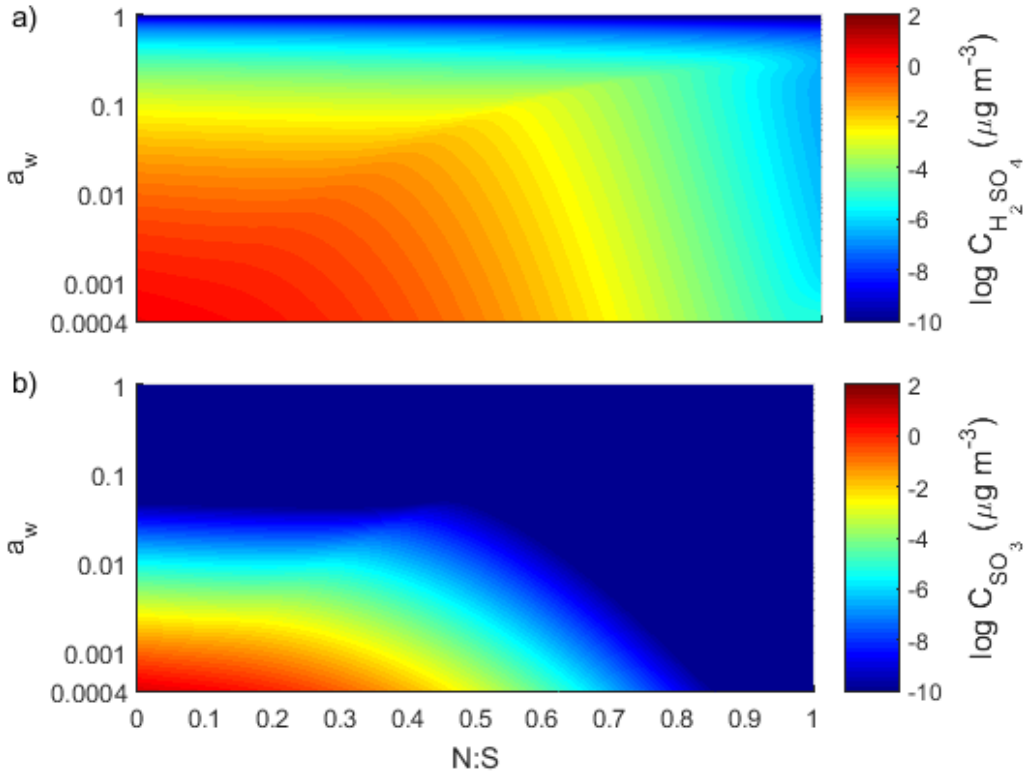

Figure S7.II. (a) The saturation concentration of H_2SO_4 $(C_{H_2SO_4,S})$ and (b) SO_3 $(C_{SO_3,S})$ in µg·m^{-3} as a function of a_w and *N:S* at *T=288.8* K. The H_2SO_4 dissociation equilibrium coefficients are $K_{H_2SO_4}$=4.00·10^9 mol kg^{-1}, and $^xK_{SO_3}$=4.55·10^{10}. For the H_2SO_4 and SO_3 pure liquid saturation vapour pressures are used parameterisations from Que *et al.* (2011) (originally from the Aspen Plus Databank).

S6 Geometrical mean diameter (GMD)

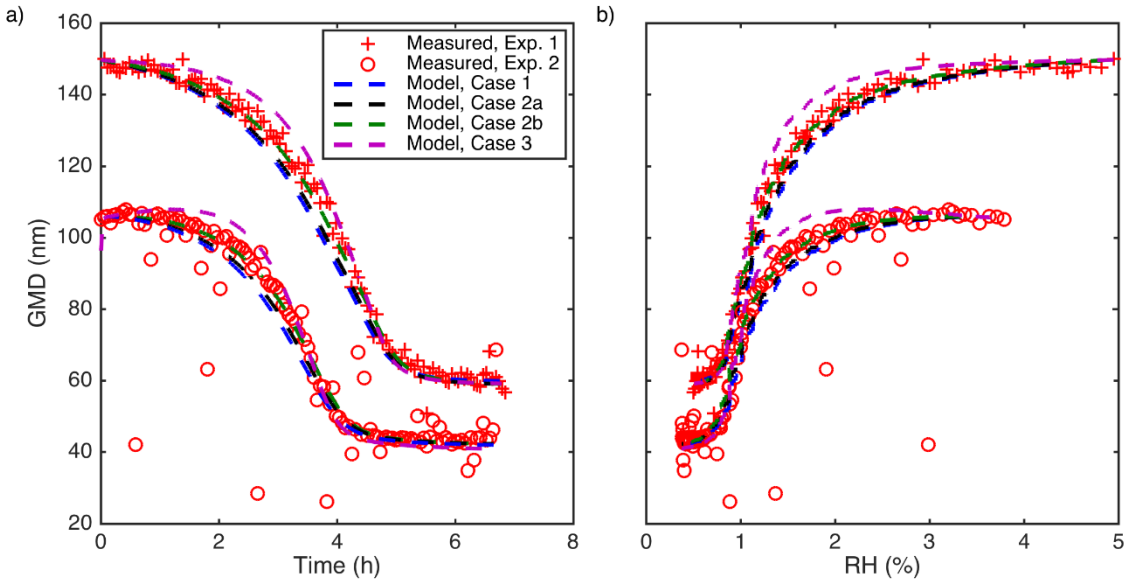

Figure S8. Measured and modelled GMD evolution as a function of (a) time and (b) RH for experiments 1 and 2 performed at *T=288.8* K. The modelled particles are composed of S(VI), H_2O and NH_3 as a particle phase contaminant. The simulations correspond to Case 1 with H_2SO_4 being the only evaporating S(VI) species, $K_{H_2SO_4}$=*3.80·10*^{9} mol·kg^{-1}, Case 2a with H_2SO_4 being the dominating evaporating S(VI) species, $K_{H_2SO_4}$=*4.00·10*^{9} mol·kg^{-1} and $^xK_{SO_3}$=*4.55·10*^{10}, Case 2b with SO_3 being the dominating evaporating S(VI) species, $K_{H_2SO_4}$ =*5.00·10*^{9} mol·kg^{-1} and $^x K_{SO_3}$ =*5.00·10*^{9} and Case 3 with SO_3 being the only evaporating S(VI) species, $K_{H_2SO_4}$=*1.00·10*^{11} mol·kg^{-1} and $^xK_{SO_3}$=*5.00·10*^{7} (see Supplement, Table S1, simulations 8–11 and 20–23). The pure liquid saturation vapour pressures of H_2SO_4 and SO_3 are calculated with parameterizations from Que *et al*. (2011) (originally from the Aspen Plus Databank).

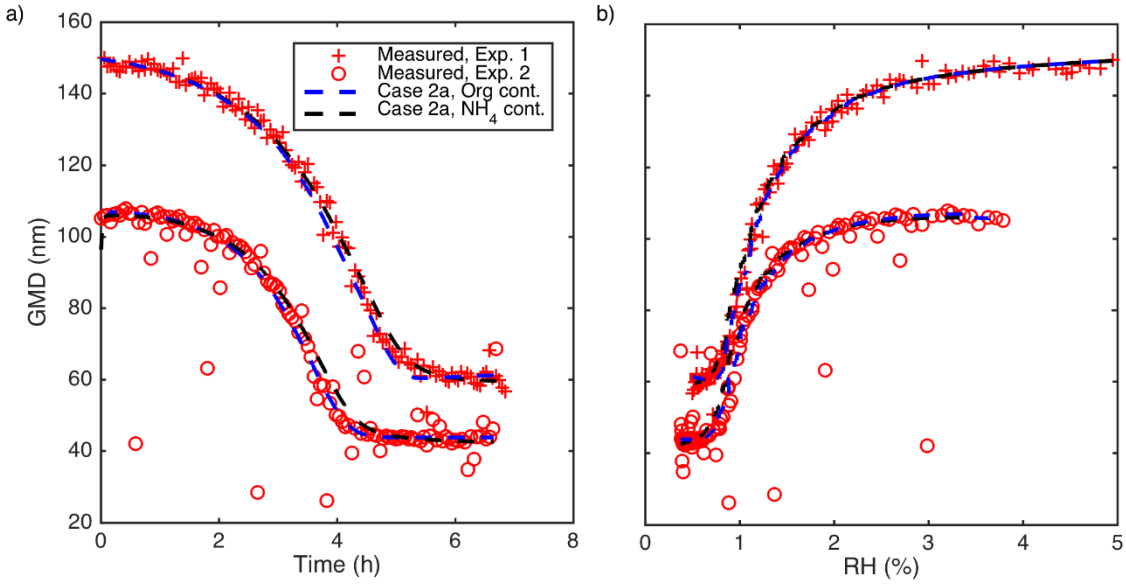

Figure S9. Measured and modelled GMD evolution as a function of (a) time and (b) RH for experiments 1 and 2 performed at *T=288.8* K. The modelled particles are composed of S(VI), H_2O and either NH3 or non–volatile, non–water–soluble organics as a particle phase contaminant for Case 2a, $K_{H_2SO_4}$=*2.40·10*^{9} mol·kg^{-1} and $^{x}K_{SO_3}$=*1.43·10*^{10} (see Supplement, Table S1, simulation 2, 6, 14 and 17). The pure liquid saturation vapour pressures of H_2SO_4 and SO_3 are taken from N–K–L, Eq. (11) and Nickless, Eq. (12) parameterizations, respectively.

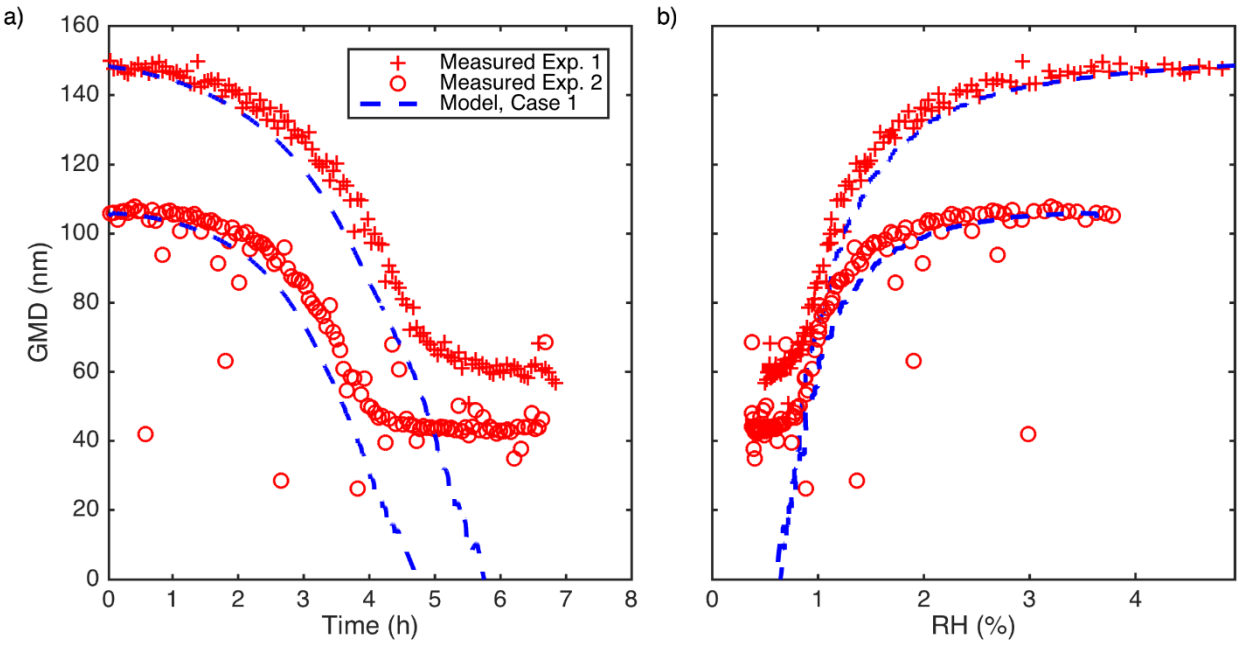

Figure S10. Modelled and measured GMD evolution as a function of (a) time and (b) RH for experiments 1 and 2 performed at *T=288.8* K. The model results presented arise from Case 1 ($K_{H_2SO_4}$=*2.00·10*^{9} mol·kg^{-1}) without any particle phase contaminant. The pure liquid saturation vapour pressure of H_2SO_4 is calculated with Eq. (11), N–K–L parameterisation.

Figure S11 compares the modelled and measured GMD evolution for experiments 1 and 2 performed at *T=288.8* K when we use the data from Giauque et al. (1960) and Eq. (15) to derive the H_2SO_4 activity. H_2SO_4 is assumed to be the only evaporating S(VI) species (Case 1), the particle phase contamination consists of non–volatile non–water–soluble organics, and the pure–liquid saturation vapour pressure of H_2SO_4 is calculated with Eq. (11) or with the Aspen Plus Databank parameterization (see Supplement, Table S1, simulations 5, 12, 19 and 24 in Table 2). The modelled GMD shrinkage agrees very well with the observations from experiments 1 and 2 when we use the tabulated H_2SO_4 chemical potential from Giauque *et al.* (1960) in combination with the pure–liquid saturation vapour pressure from the N–K–L parameterisation, Eq. (11). However, when we use the pure–liquid saturation vapour pressure parameterisation from the Aspen Plus Databank, the modelled particles evaporate earlier (at higher RH) than the observed particles. This due to ASPEN parameterisation which gives higher saturation vapour pressures compared to N–K–L parameterization.

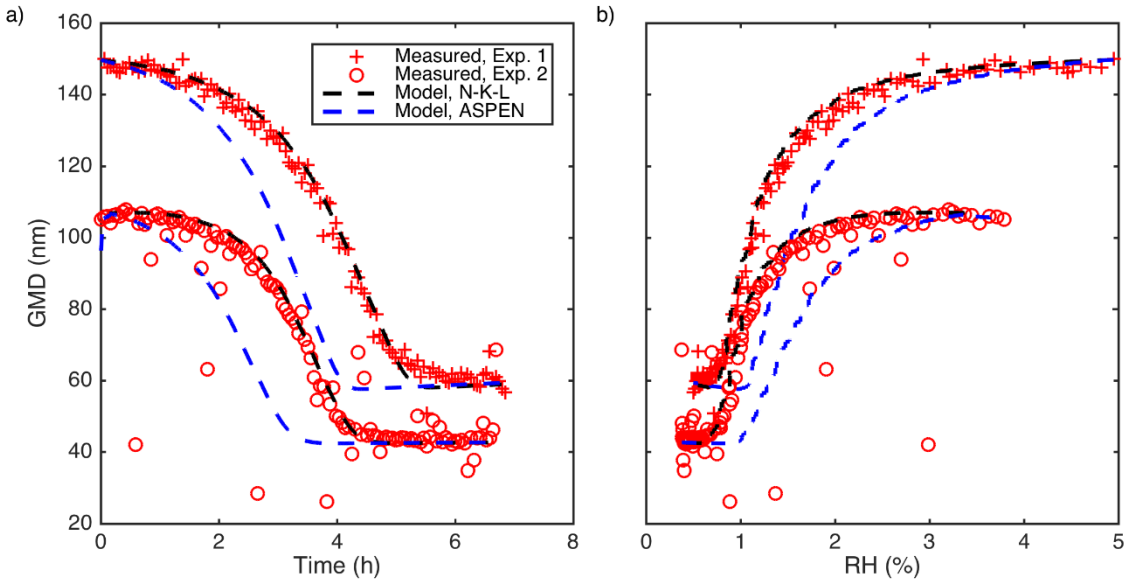

Figure S11. Measured and modelled GMD evolution as a function of (a) time and (b) RH for experiments 1 and 2 performed at *T=288.8* K. The modelled particles are composed of S(VI), H_2O and non–volatile, non–water–soluble organics as a particle phase contaminant for Case 1 (see Supplement, Table S1, simulations 5, 12, 19 and 24). The pure liquid saturation vapour pressure of H_2SO_4 is calculated with Eq. (11), N–K–L parameterisation or with parameterisation from the Aspen Plus Databank. The H_2SO_4 activity is calculated with Eq. (15) using the tabulated chemical potentials from Giauque et al. (1960).

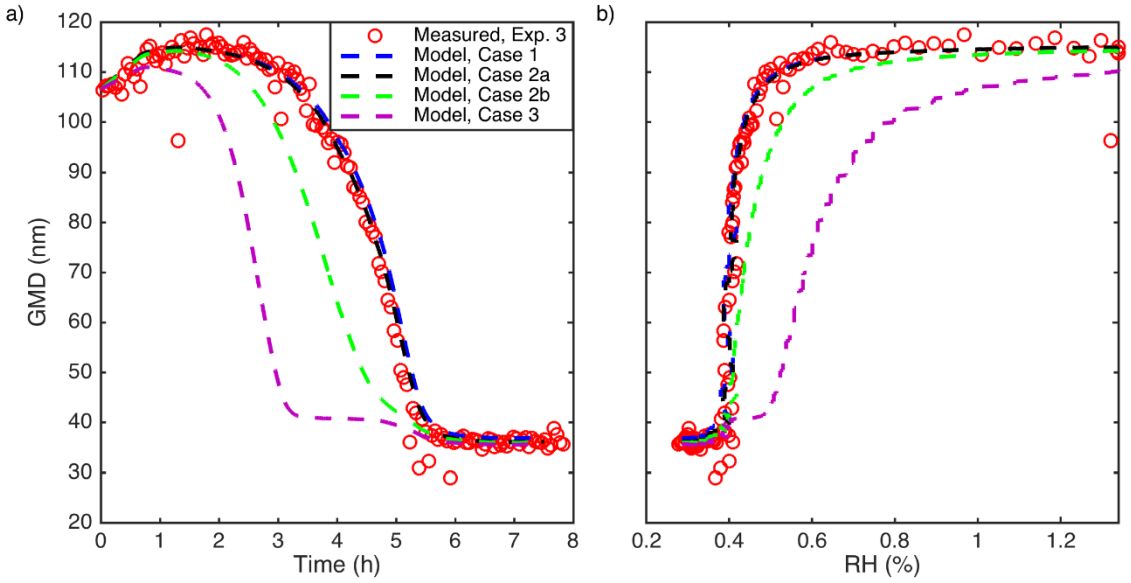

Figure S12. Measured and modelled GMD evolution as a function of (a) time and (b) RH for experiment 3 performed at a temperature range from 268 K to 293 K. The modelled particles are composed of S(VI), H_2O and NH_3 as a particle phase contaminant. The simulations correspond to Case 1, $K_{H_2SO_4}$ =3.80·10^9 mol·kg^{-1}, Case 2a, $K_{H_2SO_4}$ =4.00·10^9 mol·kg^{-1} and $^xK_{SO_3}$=4.55·10^{10}, Case 2b, $K_{H_2SO_4}$=5.00·10^9 mol·kg^{-1} and $^xK_{SO_3}$=5.00·10^9 and Case 3, $K_{H_2SO_4}$=1.00·10^{11} mol·kg^{-1} and $^xK_{SO_3}$=5.00·10^7 (see Supplement, Table S1, simulations 50-53). The pure liquid vapour pressures of H_2SO_4 and SO_3 are taken from Que et al., (2011) (original source Aspen Plus Databank).

Supplementary references

Dawson, B. S. W., Irish, D. E., and Toogood, G. E.: Vibrational spectral studies of solutions at elevated temperatures and pressures. 8. A Raman spectral study of ammonium hydrogen sulfate solutions and the hydrogen sulfate–sulfate equilibrium, *The Journal of Physical Chemistry*, *90* (2), 334–341, 1986**.**

Giauque, W. F., Hornung, E. W., Kunzler, J. E., and Rubin, T. R.: The thermodynamic properties of aqueous sulphuric acid solutions from 15 to 300 K, J. Am. Chem. Soc., 82, 62–70, 1960.

Kulmala, M. and Laaksonen, A.: Binary nucleation of water–sulfuric acid system: Comparison of classical theories with different H_2SO_4 saturation vapor pressures, J. Chem. Phys., 93, 696–701, 1990.

Massoli, P., Lambe, A. T., Ahern, A. T., Williams, L. R., Ehn, M., Mikkila, J., Canagaratna, M. R., Brune, W. H., Onasch, T. B., Jayne, J. T., Petaja, T., Kulmala, M., Laaksonen, A., Kolb, C. E., Davidovits, P., and Worsnop, D. R.: Relationship between aerosol oxidation level and hygroscopic properties of laboratory generated secondary organic aerosol (SOA) particles, Geophys. Res. Lett., 37, 5, L24801, 2010.

Myhre, C. E. L., Christensen, D. H., Nicolaisen, F. M., Nielsen, C. J. Spectroscopic Study of Aqueous H_2SO_4 at Different Temperatures and Compositions: Variations in Dissociation and Optical Properties. J. Phys. Chem. A, 107, 1979–1991, 2003.

Nickless, G.: Ed. "Inorganic Sulfur Chemistry", Elsevier, Amsterdam, 1968.

Noppel, M., H. Vehkamäki, and M. Kulmala, An improved model for hydrate formation in sulfuric–acid water nucleation, J. Chem. Phys, 116, 218–228, 2002.

Petters, M. D. and Kreidenweis, S. M.: A single parameter representation of hygroscopic growth and cloud condensation nucleus activity, Atmos. Chem. Phys., 7, 1961–1971, 2007.

Que, H., Song, Y., and Chen, C.: Thermodynamic modeling of the sulfuric acid–water–sulfur trioxide system with the symmetric Electrolyte NRTL model. J. Chem. Eng. Data, 56, 963–977, 2011.

Staples, B. R.: Activity and Osmotic Coefficients of Aqueous Sulfuric Acid at 298.15 K, J. Phys. Chem. Ref. Data, 10, 779–798, 1981.

Sullivan, R. C., Petters, M. D., DeMott, P. J., Kreidenweis, S. M., Wex, H., Niedermeier, D., Hartmann, S., Clauss, T., Stratmann, F., Reitz, P., Schneider, J., and Sierau, B.: Irreversible loss of ice nucleation active sites in mineral dust particles caused by sulphuric acid condensation, Atmos. Chem. Phys., 10, 11471–11487, 2010.

Topping, D. O., McFiggans, G. B., and Coe, H.: A curved multicomponent aerosol hygroscopicity model framework: Part 2–Including organic compounds, Atmos. Chem. Phys., 5, 1223–1242, 2005.

Zuend, A., Marcolli C., Booth , A. M., Lienhard, D. M., Soonsin, V., Krieger, U. K., Topping, D. O., McFiggans G., Peter, T., and Seinfeld, J. H.: New and extended parameterization of the thermodynamic model AIOMFAC: calculation of activity coefficients for organic–inorganic mixtures containing carboxyl, hydroxyl, carbonyl, ether, ester, alkenyl, alkyl, and aromatic functional groups, Atmos. Chem. Phys., 11, 9155–9206, 2011.